PAPER

Check for updates

Continuous flow fabrication of Fmoc-cysteine based nanobowl infused core–shell like microstructures for pH switchable on-demand anti-cancer drug delivery†

Sonika Chibh,[a] Vibhav Katoch,[a] Avneet Kour,[a] Farheen Khanam,[a] Amit Singh Yadav,[b,c] Manish Singh,[a] Gopal C. Kundu, [ID][b,c] Bhanu Prakash [ID] *[a] and Jiban Jyoti Panda [ID] *[a]

Asymmetric nanostructures such as nanobowls (NBs) can exhibit superior drug delivery performances owing to their concave structure and interior asymmetric cavities. Here, we present a facile one-step method for the fabrication of NB like structures from a mere single amino acid mimetic, *N*-(9-fluorenyl-methoxycarbonyl)-*S*-triphenylmethyl-L-cysteine following continuous-flow microfluidics enabled supra-molecular self-assembly. Following fabrication, NBs were further infused into a vesicular shell consisting of the amino acid *N*-(*tert*-butoxycarbonyl)-*S*-triphenylmethyl-L-cysteine, carrying dual acid labile groups, the triphenylmethyl and the *tert*-butyloxycarbonyl groups. The NB infused core–shell like microstructures formed after the shell coating will now be addressed as NB-shells. Presence of pH-responsive shells bestowed the core–shell NB like structures with the ability to actively tune their surface pore opening and closing in response to environmental pH switch. To illustrate the potential use of the NB-shells in the field of anticancer drug delivery, the particles were loaded with doxorubicin (Dox) with an encapsulation efficiency of 42% and Dox loaded NB-shells exhibited enhanced efficacy in C6 glioma cells. Additionally, when tested in an animal model of glioblastoma, the nanoformulations demonstrated significantly higher retardation of tumour growth as compared to free Dox. Thus, this work strives to provide a new research area in the development of well turned-out and neatly fabricated pH switchable on/off anti-cancer drug delivery systems with significant translational potential.

[a]Institute of Nano Science and Technology, Phase-10, Sector 64, Mohali, Punjab, 160062, India. E-mail: jyoti@inst.ac.in, bhanup@inst.ac.in
[b]NCCS Complex, University of Pune Campus, University Road, Ganeshkhind, Pune, Maharashtra 411007, India
[c]School of Biotechnology and Kalinga Institute of Medical Sciences (KIMS), KIIT Deemed to be University, Institute of Eminence, Bhubaneswar, 751024, India

†Electronic supplementary information (ESI) available: Details about HPLC chromatograms of the amino acids, additional details about the microfluidics fabrication process, and further results based on nanostructure characterization. See DOI: 10.1039/d0bm01386b

Introduction

The recent progress in materials and colloid science has permitted the generation of a wealth of newer nanomaterials bestowed with designed functionality and properties[1] along with tremendous application potential.[2,3] Off late, particle shape has been measured as an imperative parameter which could significantly influence the particle cellular uptake behaviour and *in vivo* fate.[4–8] In the recent past, with the advent of the development of anisotropic nanostructures such as rods[8] and nanotubes,[9] a new wave has emerged in the field of nano-

particle-mediated drug delivery and cancer nanotherapy. Nanobowls (NBs), which can be identified as dense spheres with an open upper surface, are also a class of asymmetric nanomaterials. Owing to their concave structure and interior asymmetric cavities, they hold the ability to exhibit superior performances in effective drug delivery.[10]

Currently, the most common methods being used for the production of particles with asymmetric and controllable morphology include spray-drying,[11] layer-by-layer fabrication,[12] freeze-drying[13] and solvent evaporation.[14,15] However, most of these are based on template-oriented strategies or involve tedious and time-consuming multi-step protocols. This warrants the development of alternative and simple one-step procedures for the production of asymmetric nanostructures. Recently, self-assembly that relies on the natural propensity of molecules to be amassed together and form supramolecular structures has turned out to be an important strategy to produce a plethora of nanostructures with desirable properties together with a varied range of shapes and sizes. A number of self-assembled systems such as micelles[16,17] and vesicles[18] have been developed from a variety of biomolecules such as

proteins, carbohydrates, and nucleic acids.[19] These self-assembled structures have demonstrated wide-spread applications in the fields of drug delivery,[20] bioimaging,[21] gene therapy[22] and vaccine development.[23] Among biomolecules, peptides have been shown to serve as an important class of self-assembling building blocks and additionally single amino acids have also been used as monomers towards constructing a plethora of self-assembled nanostructures.[24–26]

Despite remarkable achievements in self-assembly based research, the fabrication process of self-assembled nanostructures still requires further developments in terms of achieving controlled parameters such as their shape, size and polydispersity. Though the process can be controlled by pre-determining specific parameters such as the type of material (amino acids/peptides/polymers), their hydrophilicity and hydrophobicity, and the type of solvent used, the main concern which still prevails and demands attention is the control over specific particle parameters such as size, shape, polydispersity and composition.

In the conventional bulk production method of self-assembled materials, it has been observed that the local environment cannot be controlled well, which leads to the production of a heterogeneous population of particles. The bulk mixing method generally lacks a precise control over various nanostructured parameters such as the size, shape and loading efficiency.[27,28] In the recent past, tremendous efforts have been made in this direction of further optimizing these self-assembled particle parameters. In this context, microfluidics, which actually involves manipulating a minimal volume of fluid (between tens to hundreds of micrometres) in a con-

fined microspace, has emerged as a technological alternative for the production of self-assembled structures with precisely controlled parameters.[29] A microfluidic based platform can act as a powerful tool to fabricate self-assembled structures with essential features by keenly manipulating the minute details of their structure–performance relationships.[30] When using microfluidic based synthesis, particle size can be conveniently tuned by altering the flow parameters in the microfluidic channel. Furthermore, it enforces a precise control over the particle's morphological properties owing to the fast diffusion and enhanced heat and mass transfer mechanism achieved in a microchannel environment.[31]

Building on all these aspects, here in this study, we established a new synthesis route for the formation of amino acid-based core–shell nanobowl microstructures (NB-shells) using the flow fabrication method. A smart nanocomposite core–shell encapsulation system based on the amino acid mimetic, N-(9-fluorenylmethoxycarbonyl)-S-triphenylmethyl-L-cysteine (Fmoc-Cys(Trt)-OH), self-assembled into NBs as the drug loading core along with a pH-responsive vesicular shell composed of N-(tert-butoxycarbonyl)-S-triphenylmethyl-L-cysteine (Boc-Cys(Trt)-OH) is described here (Scheme 1). These NBs with their hollow interior cavities were further explored as stimulus-responsive carriers of anti-cancer drugs in animal tumor models. The presence of an empty core in the NBs offered advanced delivery and encapsulation possibilities for drug molecules, and they are protected from hydrolysing body fluids until the encapsulated molecules experience triggered release at the desired site.

To the best of the authors' knowledge, there is no report to date on the formation of NBs using single amino acid-based
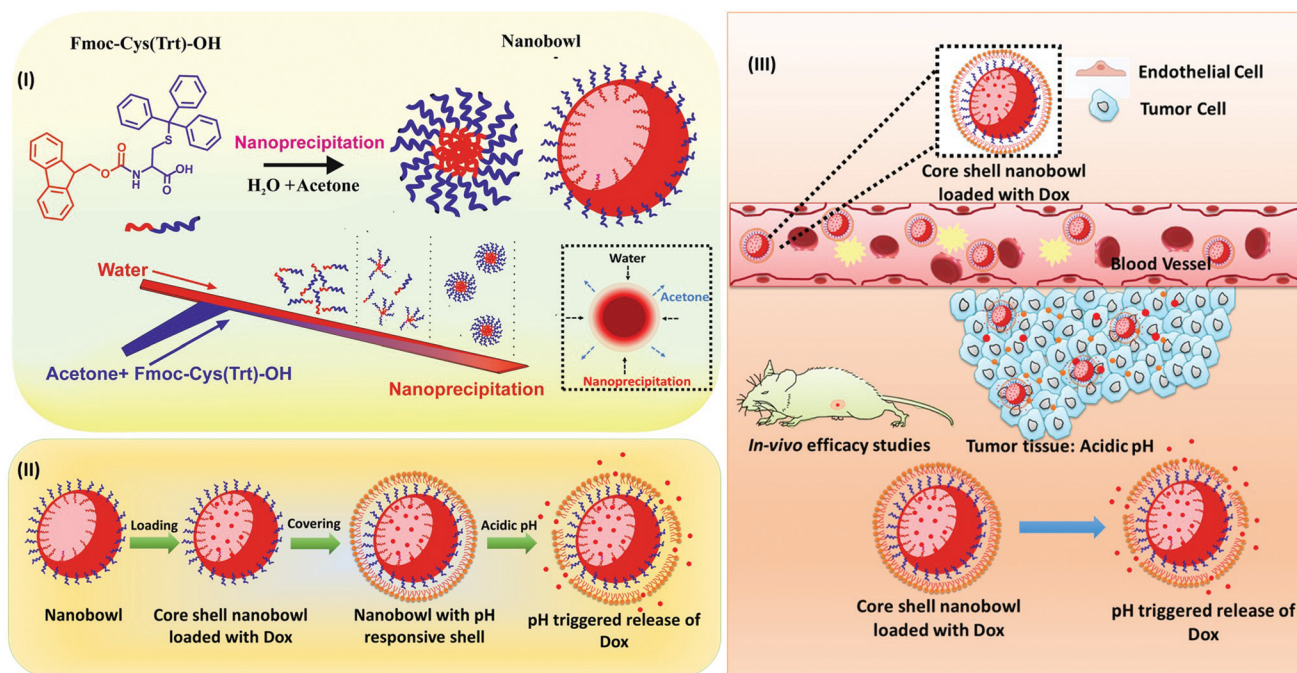
Scheme 1 Overall scheme showing the formation of the core−shell nanobowl-microstructures (NB-shells) and their application in on-demand tumor drug delivery.

self-assembly *via* a microfluidics-based approach. Furthermore, there are in fact only a couple of reports to date, which shed light on the development of stimulus-responsive hollow polymer-based shape tunable particles as smart carriers for externally triggered drug release concerning a variation in the pH or redox environment.[32,33] Hence, the pH responsive hollow or porous particles described herein can serve as a new and exciting platform for stimuli activated drug delivery applications.

Results

Synthesis and characterization of nanostructures generated through the microfluidics-based approach

The current work has outlined a method to form NBs using a single amino acid-based monomer following a microfluidics-based synthesis approach (Scheme 2). The microfluidic setup used a soft lithography-based technique (Fig. S1†) for the fabrication of microchannels of 100 μm diameter using PDMS (Fig. S2†).

We tuned various parameters such as the flow rate ratio (FRR) (1 : 2 and 2 : 3 of organic phase : aqueous phase), total flow rate ratio (TFR: 1, 2, and 3 mL min^{-1}) and concentration of amino acids (0.1 mg mL^{-1}, 0.25 mg mL^{-1} and 0.5 mg mL^{-1}) at room temperature in order to produce desirable structures. In the case of Boc-Cys(Trt)-OH, dynamic light scattering (DLS) revealed that the particles had an average hydrodynamic diameter (d, nm) of 542 ± 9.24 nm at 0.1 mg mL^{-1}, 439 ± 11.2 nm at 0.25 mg mL^{-1} and 373 ± 10.64 nm as the concentration was increased to 0.5 mg mL^{-1} (Fig. 1A and Table 1). We also tried to determine the uniformity of the particle solution using its polydispersity index (PDI) as an indicator as shown in Table 1.

As a reference, particles were also synthesized following a bulk mixing method using the same amino acid with a similar ratio of the organic solvent to water (2 : 3). In this case, the mean hydrodynamic diameter of the particles was observed to be smaller than that of the particles formed by the microfluidics-based approach. The diameters in this case were found to be 243 ± 13.14 nm, 279 ± 15.2 nm and 285 ± 9.81 nm (Fig. 1A and Table 1) with PDI values of 0.28, 0.14 and 0.71 at amino acid concentrations of 0.1 mg mL^{-1}, 0.25 mg mL^{-1} and 0.5 mg mL^{-1}, respectively.

A parallel study of the microfluidics-based synthesis of the particles was carried out by using a modified analogue of the amino acid, Fmoc-Cys(Trt)-OH, with a Fmoc group at the N-terminus in place of the Boc group. It was observed that the particles formed had a mean hydrodynamic diameter of 542 ± 15.2 nm at a concentration of 0.1 mg mL^{-1}, 468 ± 11.24 nm at a concentration of 0.25 mg mL^{-1} and a size of 1422 ± 17.21 nm at 0.5 mg mL^{-1} (Fig. 1B and Table 1). As a reference, particles were also formed following bulk mixing under similar conditions. It was observed that using a manual synthesis strategy, the amino acid mimetic formed particles with mean hydrodynamic diameters of 750 nm ± 18.21, 791 ± 11.24 nm and 743 ± 17.24 nm (Fig. 1B and Table 1) at amino acid concentrations of 0.1 mg mL^{-1}, 0.25 mg mL^{-1} and 0.5 mg mL^{-1}, respectively. Thus, a concentration-based variation in particle size was clearly observed.

Characterization of particles using scanning electron microscopy (SEM)

The prepared particles were next evaluated by SEM for morphological and surface topological analysis (Fig. 2A). In the case of Boc-Cys(Trt)-OH, no proper formation of particles was observed at concentrations of 0.1 mg mL^{-1} and 0.25 mg mL^{-1} as shown in Fig. 2B; however, vesicle-like particles were formed at a concentration of 0.5 mg mL^{-1}. Similar behavior was observed in the case of particles synthesized through the
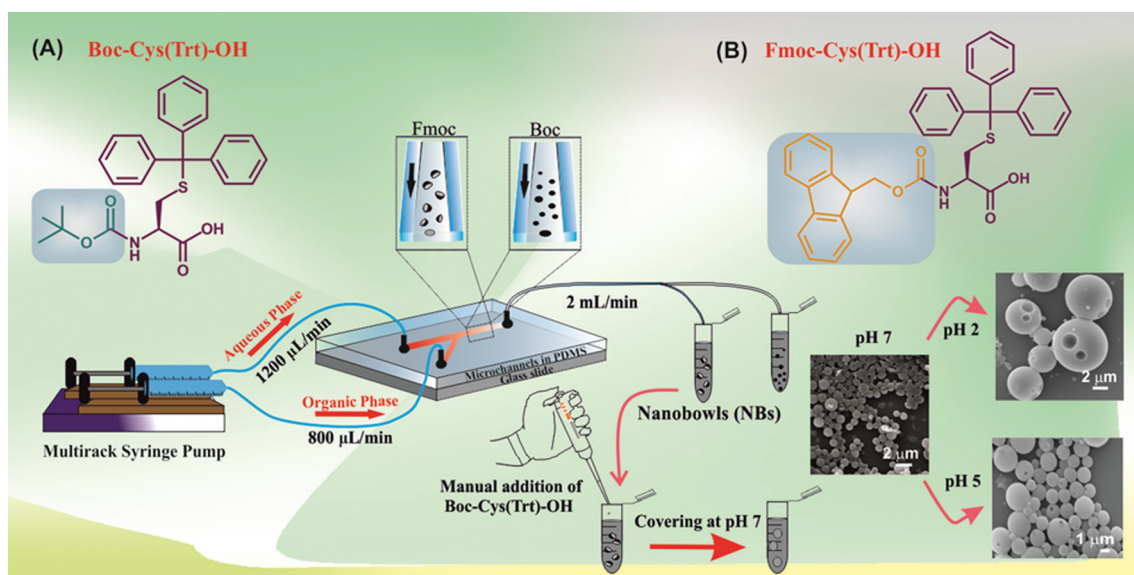
Scheme 2 Overall scheme demonstrating the process of NB formation using the microfluidic-based approach.

(A)

Manual

Microfluidics

(B)

Manual
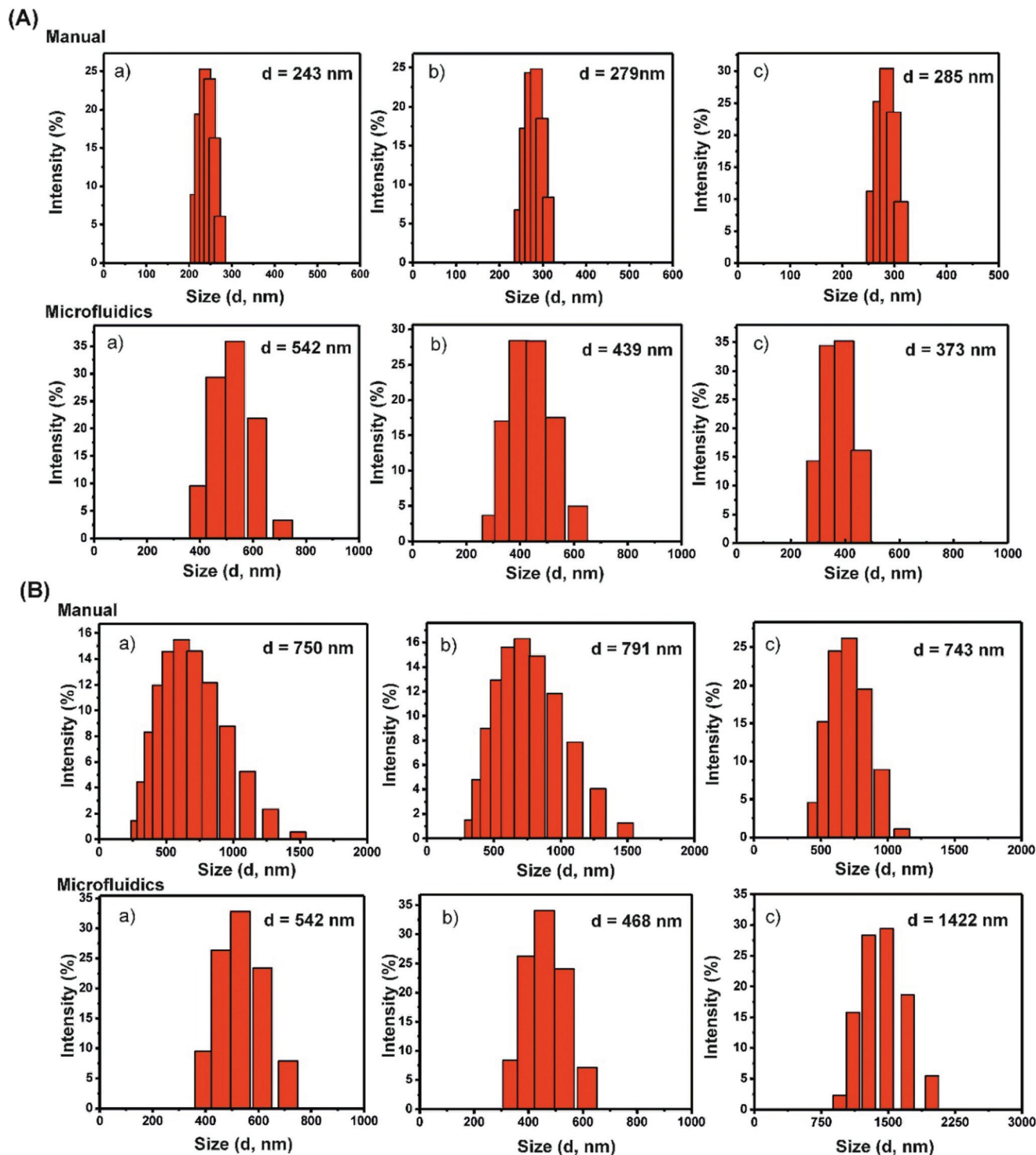
Microfluidics

Fig. 1 Size distribution graphs of the amino acid derived particles synthesized using manual and microfluidics-based methods at different concentrations of amino acids of 0.1 mg mL^{-1}, 0.25 mg mL^{-1} and 0.5 mg mL^{-1} respectively, as measured by DLS. (A) Intensity distribution profiles of particles formed using Boc-Cys(Trt)-OH *via* manual and microfluidics methods and (B) intensity distribution profiles of particles formed using Fmoc-Cys(Trt)-OH *via* manual and microfluidics methods.

bulk mixing method. It was further observed that by following the microfluidics-based approach, Fmoc-Cys(Trt)-OH formed discrete NBs, at a concentration of 0.5 mg mL^{-1} (Fig. 2C). These NBs had a mean size of 810 ± 30 nm. Though, the for-

mation of NBs was also evident at lower concentrations of, 0.1 mg mL^{-1} and 0.25 mg mL^{-1}, their density was much less as compared to the ones observed at a concentration of 0.5 mg mL^{-1}. Some vesicle-like particles also co-existed with

Paper

Biomaterials Science

Table 1 Particle size and PDI of particles prepared using Boc-Cys(Trt)-OH and Fmoc-Cys(Trt)-OH showing a comparison of manual and microfluidics methods

| | Boc-Cys(Trt)-OH | | | | Fmoc-Cys(Trt)-OH | | | |
| | Manual | | Microfluidics | | Manual | | Microfluidics | |
Conc. (mg mL⁻¹)	Size (nm)	PDI	Size (nm)	PDI	Size (nm)	PDI	Size (nm)	PDI
0.1	243	0.28 ± 0.01	542	0.06 ± 0.015	750	0.09 ± 0.008	542	0.26 ± 0.07
0.25	279	0.14 ± 0.006	439	0.06 ± 0.009	791	0.13 ± 0.01	468	0.30 ± 0.09
0.5	285	0.71 ± 0.02	373	0.97 ± 0.12	743	0.05 ± 0.009	1422	0.16 ± 0.08

the NBs as observed in the SEM micrographs. We also identified that 2 : 3 FRR, 2 mL min⁻¹ TFR and 0.5 mg mL⁻¹ of amino acid together served as the most appropriate condition for the formation of bowl-shaped particles using Fmoc-Cys(Trt)-OH. To our surprise, the self-assembly of the amino acid mimetic when carried out using manual-mixing method resulted mostly in spherical structures [Fig. 2C; 3A (a)] rather than bowls [Fig. 2C and 3 A (b)].

By further using SEM analysis, it was clearly distinct that the bowl-shaped particles mostly falling in the nanorange (nanobowls; NBs), were formed in the case of Fmoc-Cys(Trt)-OH (Fig. 2C) and in the case of Boc-Cys(Trt)-OH, mostly spherical structures were observed (Fig. 2B). Keeping in view the uniqueness of these bowl-shaped structures, further studies in the manuscript were carried out using these bowl-shaped nanoparticles only.

Further validation of the formation of NBs using atomic force microscopy (AFM) and transmission electron microscopy (TEM)

Further investigation of the morphology of the particles was carried out using TEM and AFM. A comparative study between the structures fabricated using the microfluidics-based approach and the structures formed using the manual mixing method was performed. Formation of NBs was only evident in the case of structures synthesized by the microfluidics-based approach as shown in Fig. 3A(b) and B(b). TEM images demonstrated the formation of spherical structures with a dark interior by Fmoc-Cys(Trt)-OH, which might have resulted due to the flattening of the NBs under high vacuum conditions in TEM. TEM images further confirmed the formation of hollow core–shell like structures by the amino acid mimetic. These structures had a mean inner core diameter of 396 ± 20 nm. On the other hand, in the case of the manual fabrication method, formation of spherical particles was evident as shown in Fig. 3B(a).

Furthermore, the formation of NBs was also ascertained using AFM (Fig. 3C). Tapping mode AFM carried out for the nanostructures demonstrated the formation of NBs having a mean diameter of 346 ± 24 nm [Fig. 3C(a)] with a color contrast image as shown in Fig. 3C(b).

Additionally, in order to confirm the hollow cavity like nature of the NBs, the bowls were further loaded with polystyrene microbeads. Fig. S3† shows a typical example where the NBs when co-dispersed with 300 nm polystyrene solid beads demonstrated the presence of the beads inside the bowl cavity.

Covering of the NBs with a pH responsive shell

After their formation, NBs were covered with a shell consisting of the amino acid Boc-Cys(Trt)-OH. The amino acid shell could successfully cover the NBs at pH 7, and the selective removal of the Boc and Trt groups under acidic conditions (pH 2 and pH 5) was expected to form pores in the shell for achieving acid-triggered drug release. The confirmation of the covering on the NBs was further done using SEM analysis (Fig. 4A). SEM images revealed that the nano-bowl like particles were homogeneously covered with a shell. After the shell covering, a complete spherical microstructure was observed, termed henceforth as NB-shells. Further characterization of the NB-shells was performed using AFM. As expected, an increment in the height profile of the NB-shells was observed as shown in Fig. 4B.

DLS and stability studies of NB-shells

DLS studies performed to determine the size of NB-shells showed the formation of particles with a mean size of 1496 nm. Stability studies of NB-shells were also performed using DLS for a period of 48 h. Results demonstrated that the particles were stable with not much variation in their mean particle size during this period of observation (Fig. S4†).

As a control, we also tried covering the NBs with Fmoc-Cys(Trt)-OH, but could not get an uniform covering, rather many uncovered NBs with altered size and shapes were observed (Fig. S5†).

pH responsiveness of NB-shells

Next, the pH responsiveness of the NB-shells was investigated by incubating them under acidic conditions (pH 5 and 2) (Fig. 5A and B). SEM analysis revealed the formation of few pores when the NBs were incubated at acidic pH 5, whereas multiple pores were observed at pH 2.

Confirmation of acid triggered amino acid degradation using high performance liquid chromatography (HPLC) analysis

We hypothesized that the opening of pores at acidic pH was due to the cleavage or deprotection of the acid labile groups, triphenylmethyl (-trt) and *tert*-butoxycarbonyl (-Boc), from the amino acid Boc-Cys(Trt)-OH. This was confirmed by carrying out combined analytical HPLC and mass spectrometric analysis. HPLC chromatograms and their corresponding mass peaks and analysis of the results are presented in Fig. S6a–c.†
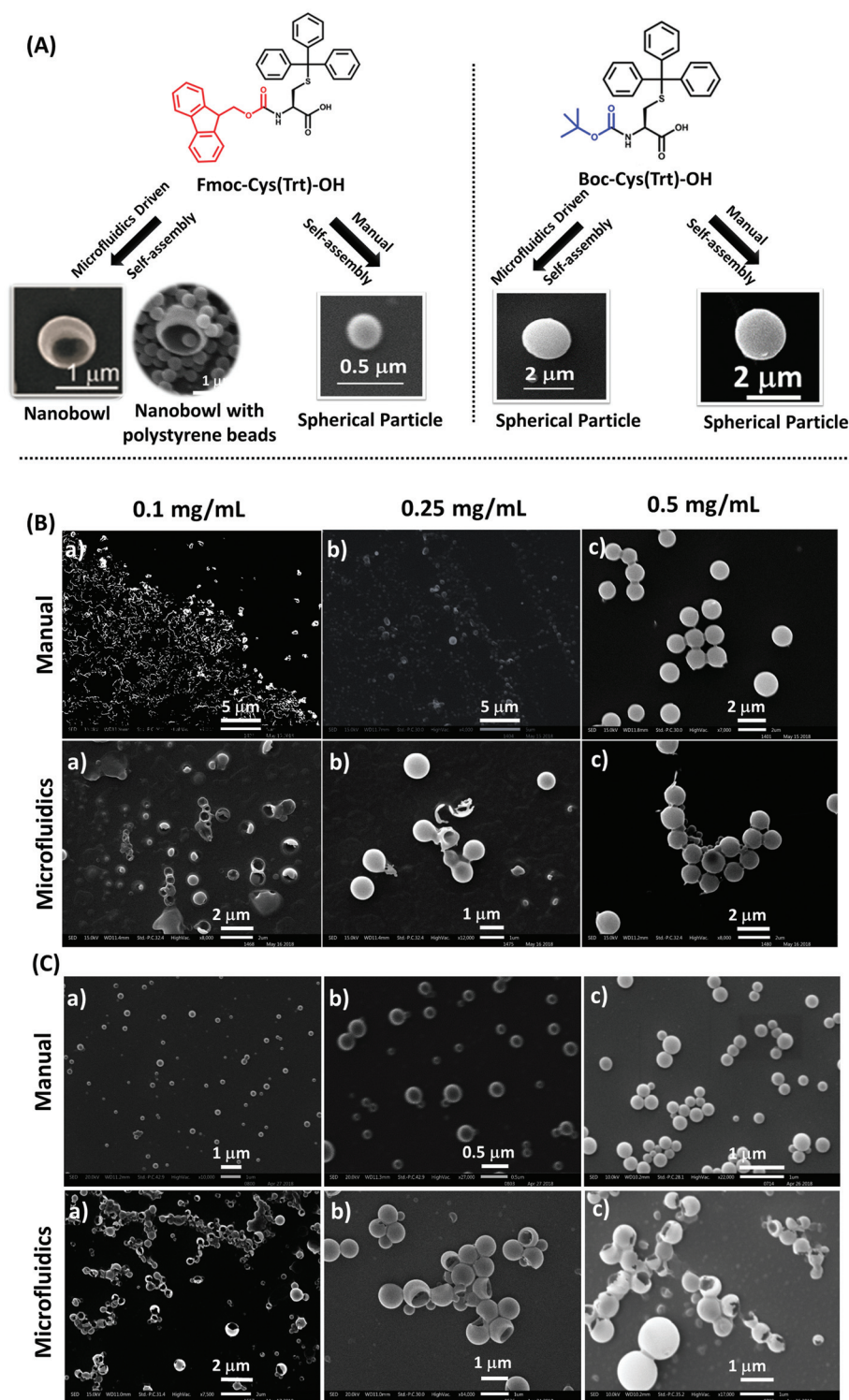
Fig. 2 (A) Scheme representing the formation of particles using Fmoc-Cys(Trt)-OH and Boc-Cys(Trt)-OH *via* microfluidics and manual self-assembly methods. (B) and (C) SEM images of the particles prepared at different concentrations (0.1 mg mL^{-1}, 0.25 mg mL^{-1} and 0.5 mg mL^{-1}) of amino acids using manual and microfluidics-based methods, respectively. (B) Particles formed using Boc-Cys(Trt)-OH and (C) particles formed using Fmoc-Cys(Trt)-OH. At a concentration 0.5 mg mL^{-1}, nano-size-range particles with a smooth surface and a hole (nanobowls) were observed.
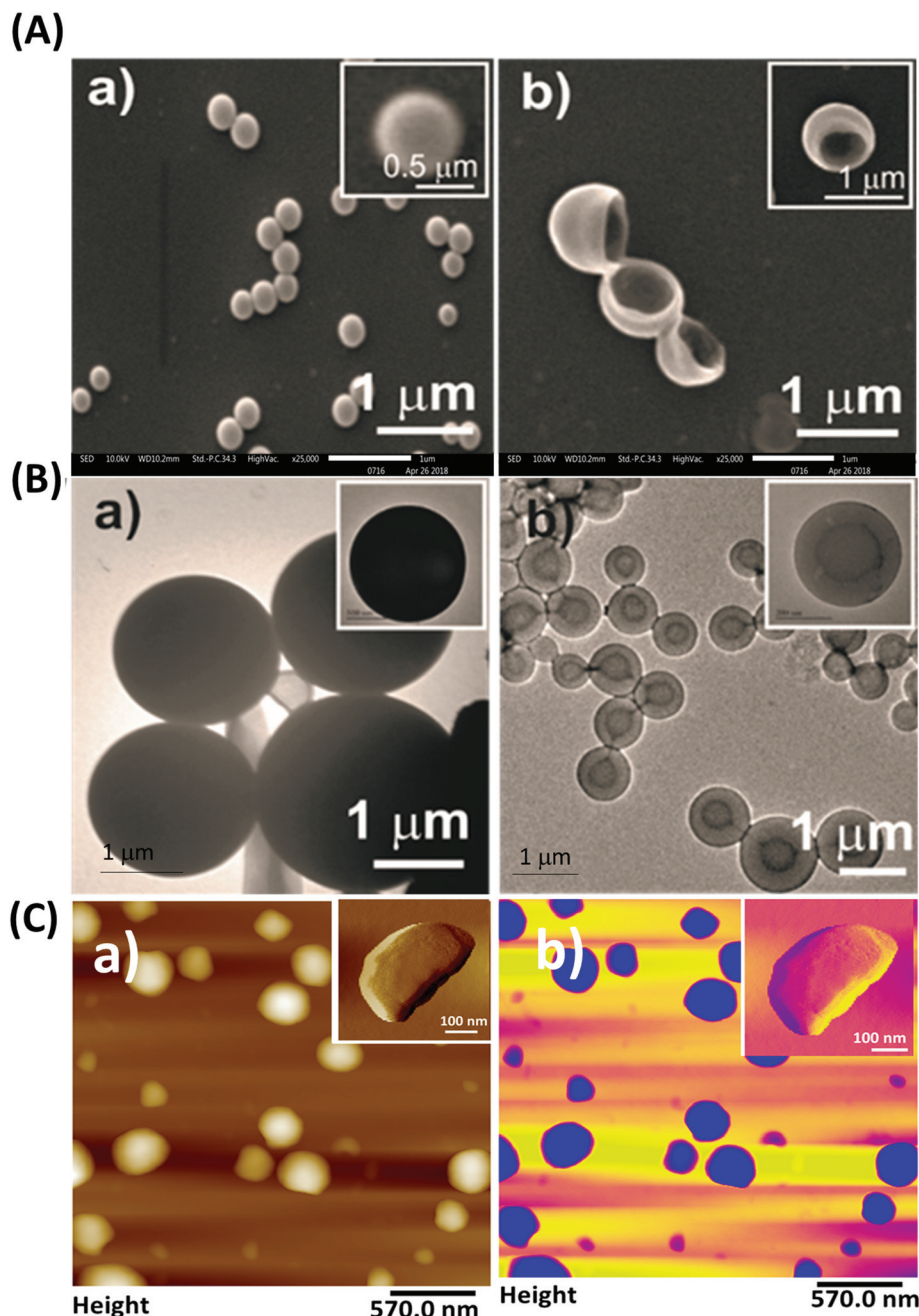
Fig. 3 (A) SEM images of particles synthesized following (a) manual (inset showing a zoomed image of a spherical particle) and (b) microfluidics (inset showing a zoomed image of a NB) based approaches by using Fmoc–Cys(Trt)–OH as the monomer. (B) A comparison between the TEM images of the particles synthesized following (a) manual (inset representing the zoomed image of a spherical particle) and (b) microfluidics (inset depicting the zoomed image of a NB) based approaches by using Fmoc–Cys(Trt)–OH as the monomer is presented. (C) AFM image and color contrast image (inset showing a zoomed image of a NB) of NBs prepared using the microfluidics method are shown as (a) and (b) respectively.

Encapsulation of Dox in NB-shells and a study presenting its release behaviour from the structures under different pH conditions

Bowl-shaped structures owing to their unique shape can act as excellent platforms as drug carriers.[10,34] By controlling various assembly parameters such as the flow rate ratio and total flow rate in the microfluidic setup, one can master a better control over the loading of drug molecules inside the particles. To determine the potential applicability of NBs for drug delivery applications, the anti-cancer drug Dox was encapsulated in the NBs online during the microfluidics-based flow synthesis.
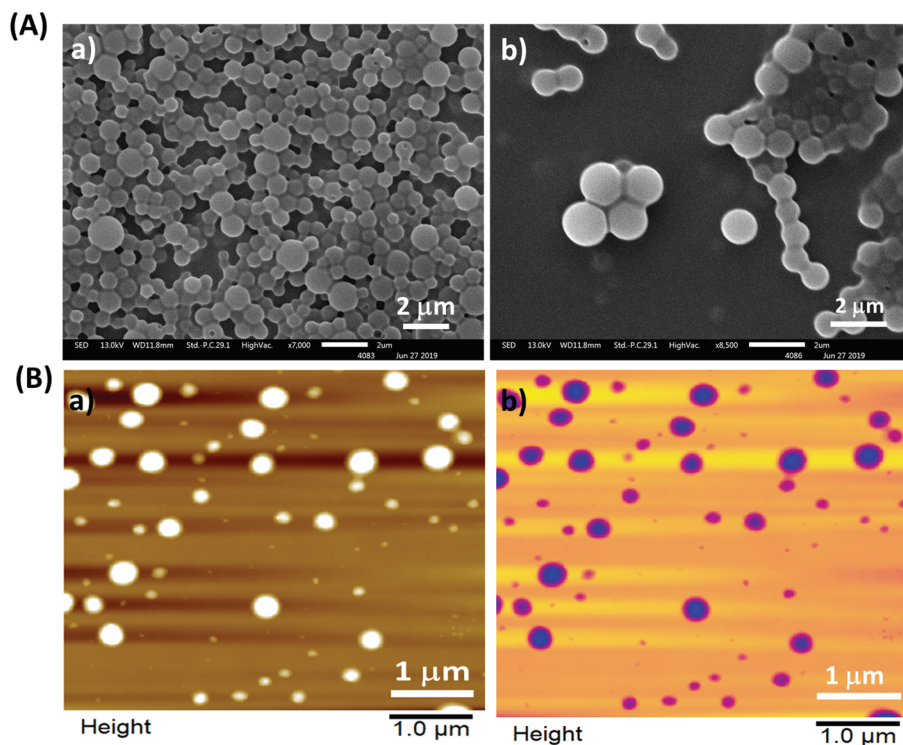
Fig. 4 (A) SEM analysis of NB-shells at pH 7. (a) SEM images of the concentrated sample and (b) 5× diluted sample. A complete covering on the NBs was observed. (B) (a) AFM analysis of the NB-shells and (b) NB-shells demonstrated a change in color at the edges confirming shell coating.
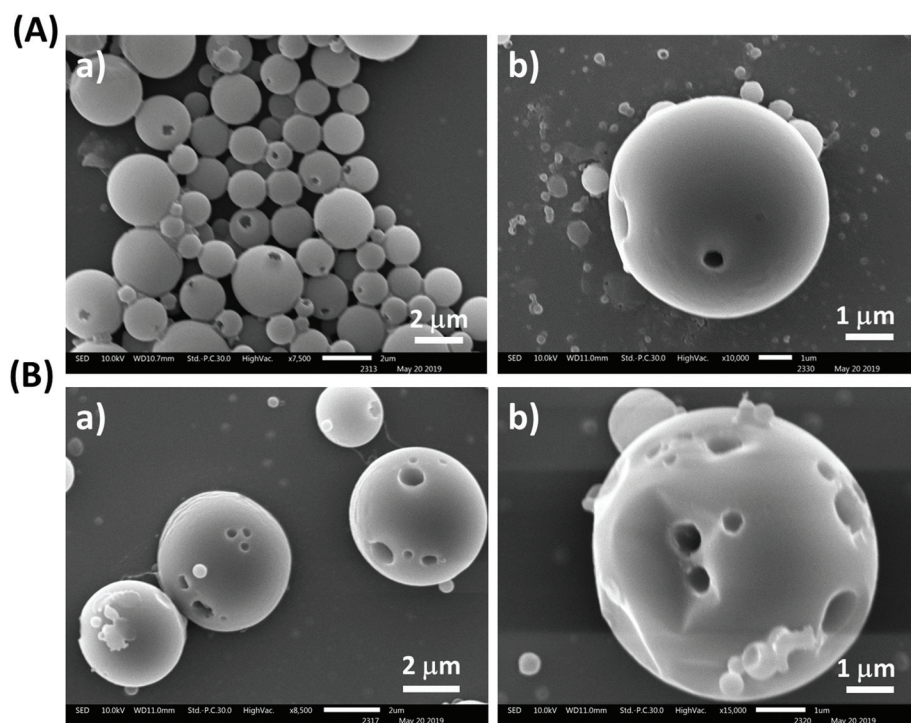
Fig. 5 (A) (a) SEM analysis demonstrating the opening of NB-shell-pores at pH 5. (b) Zoomed image of the pore opening at pH 5. (B) (a) At pH 2, multiple pores were formed on the NB-shells as is evident in the figure and (b) zoomed image of the porous NB-shells observed at pH 2.
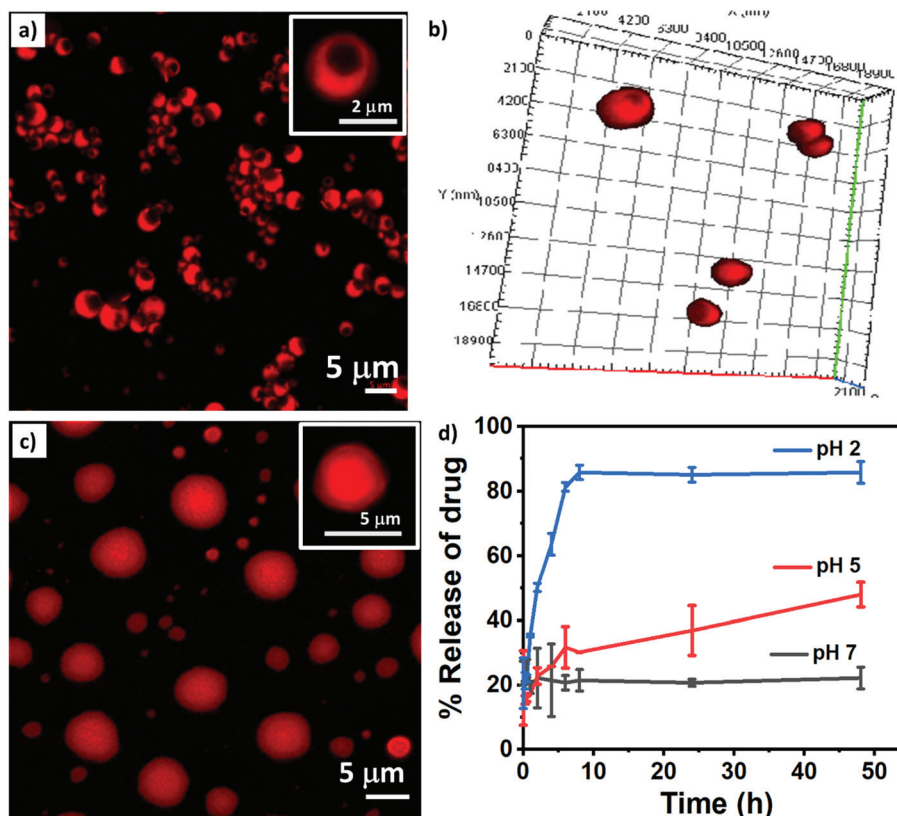
Fig. 6 Confocal images depicting positive drug loading (a) in the NBs, (b) 3D image of Dox loaded NBs, (c) confocal images of Dox loaded NB-shells at pH 7 and (d) release profile of Dox from NB-shells determined up to 48 h at pH 7, pH 5 and pH 2.

Drug-loaded particles were further characterized using DLS and confocal microscopic studies.

Confocal microscopic images of Dox loaded NBs confirmed the encapsulation of the drug in the NBs (Fig. 6a). A 3D image (Fig. 6b) and images taken at different depths of the particles (Fig. S7†) using confocal microscopy to confirm the formation of bowl-shaped structures are shown here. The drug demonstrated a percentage encapsulation of almost 42% in the NBs. After being loaded with Dox, the NBs demonstrated a mean size of approximately 1766 ± 52 nm, as observed under a confocal microscope. A clear rim like boundary covering the interior core is also visible confirming the core–shell like structure.

After the NBs were loaded with drug molecules, they were further coated with a shell composed of the pH responsive amino acid Boc-Cys(Trt)-OH to form Dox loaded NB-shells. Fig. 6c demonstrates the confocal image of the drug loaded NB-shells. Confocal microscopic images clearly depicted positive loading of the drug in the structures as the red fluorescence exhibited by the structures emanate from the entrapped Dox molecules.

After the confirmation of drug loading in the NB-shells at pH 7, the pH of the sample was changed to 5 (Fig. S8a†) and 2 (Fig. S8b†). This was done to validate the pH-based stimuli responsive nature of the NB-shells. Confocal microscopic

studies at pH 5 and pH 2 further indicated towards the pH triggered opening of the pores of the drug loaded and pH responsive amino acid NB-shells.

In order to establish stimuli triggered release of the encapsulated drug Dox from the NB-shells, drug release studies were performed for the particles at pH 7, pH 5 and pH 2, for a period of 48 h. As shown in (Fig. 6d) no release of the drug was observed at pH 7, whereas upon exposure to acidic conditions, a rapid surge in Dox release up to 40–45% and 85–90% was observed at pH 5 and pH 2, respectively, within 48 h. This release could be explained by the pH-induced opening of pores in the acidic environment, whereas the absence or significantly less release of the drug from the particles at pH 7, due to the intact coating of the bowl-shaped particles, was evident.

Cellular uptake studies

In order to act as a carrier for the therapeutic molecules, it is important that the particles should have the ability to move inside the cells and gain access to the internal cellular milieu. In order to validate the cell delivery potential of NB-shells, cellular uptake studies were carried out in C6 glioma cell lines. The cells were incubated with the Dox loaded NB-shells and their uptake was analysed using confocal microscopy. Images demonstrated enhanced fluorescence

intensity in the case of drug-encapsulated particles as compared to free Dox (Fig. 7A). Quantitative estimation of cellular uptake, determined through Zen blue LSM 880 software to further support the confocal images, demonstrated a higher intensity in the case of the NB-shells as compared to the bare drug signifying enhanced cellular uptake in the case of NB-shells (Fig. S9a†). It was observed that, NB-shells demonstrated approximately 4-fold higher fluorescence intensity *vs.* free Dox.

Efficacy studies in glioma cells

Furthermore, the anti-proliferative effect of Dox on C6 glioma cells was determined by performing MTT assay. Prior to this, cytotoxicity experiments were carried out with void NB-shells in order to address the biocompatibility of the particles. As shown in Fig. S9b,† approximately 94–95% of cells were viable following treatment with bare particles. Further efficacy studies of the drug loaded NB-shells were performed in C6 cells at various concentrations ranging from 2.5 μg mL^{-1} to
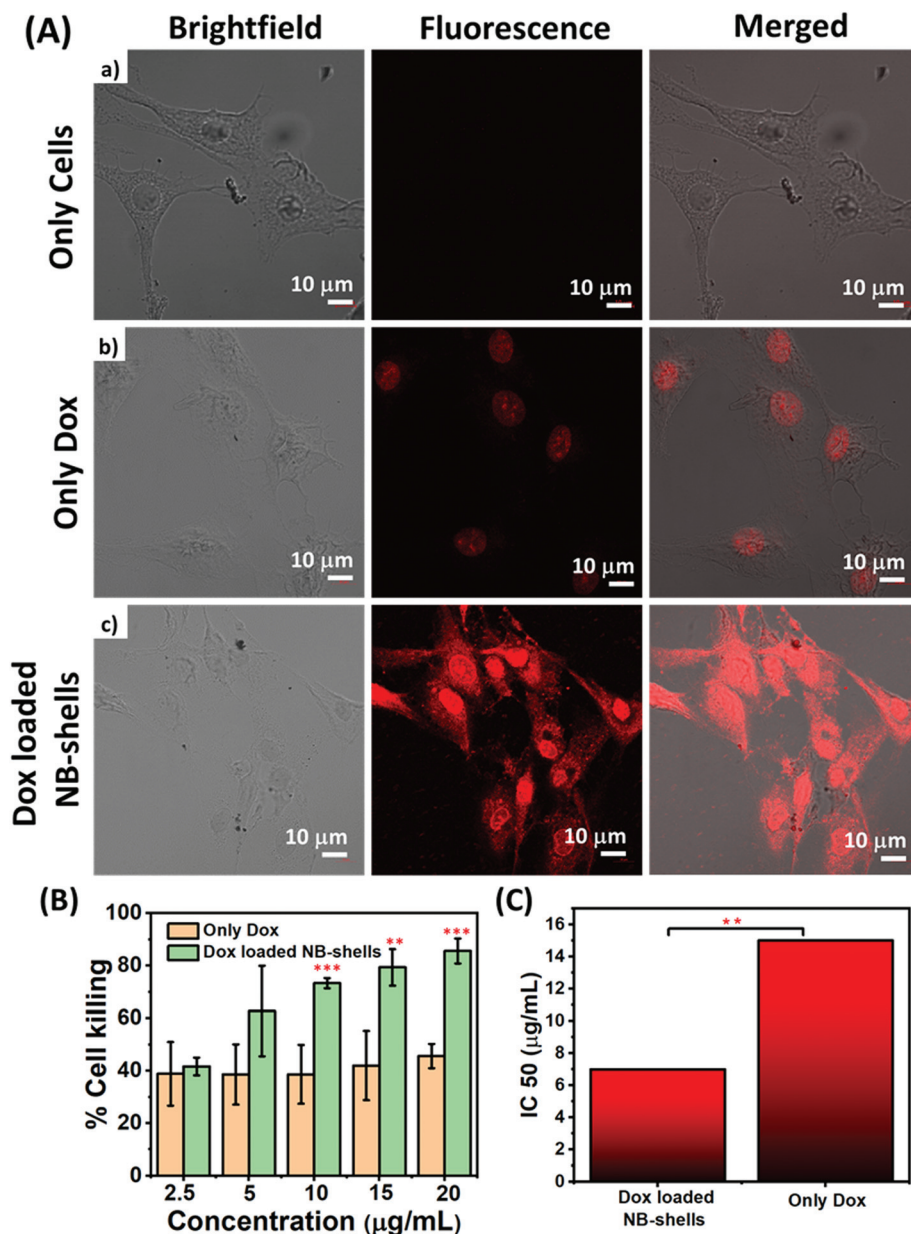
Fig. 7 (A) Cellular uptake study of Dox loaded NB-shells in C6 cells. (B) *In vitro* efficacy of Dox loaded NB-shells and only Dox against C6 cells, showing enhanced efficacy in the case of NB-shells loaded with the anti-cancer drug as compared to the free drug. (C) Graph showing the IC$_{50}$ values of Dox and Dox loaded NB-shells. Data reported as the mean of three values, (n = 3) ± SD. *** and ** represent the levels of significance ($P <$ 0.001 and $P <$ 0.01, respectively).

20 µg mL^{-1} over a period of 24 h. Results of MTT assay demonstrated that Dox loaded NB-shells significantly diminished the cellular viability of C6 cells as compared to free Dox (Fig. 7B). Cytotoxicity studies further revealed that free Dox exhibited an IC$_{50}$ value of 15 µg mL^{-1}, whereas Dox loaded NB-shells exhibited an IC$_{50}$ of 6.6 µg mL^{-1} (Fig. 7C). IC$_{50}$ values revealed that bowl-shaped particles with Dox had significantly higher efficacy in terms of their IC$_{50}$ values that was almost 2.3-fold less as compared to native Dox suspension.

In vivo anti-tumor efficacy studies

Next the therapeutic efficacy of Dox-loaded NB-shells was determined in glioma xenografts. Efficacy was examined by determining the tumour size after intra-tumoral injections of the formulations every alternate day. In brief, tumor growth was induced by subcutaneous injection of C6 cells in the dorsal right flank of NOD/SCID mice. The animals were treated with void NB-shells, Dox alone and Dox loaded NB-shells. Mice bearing glioma tumours were randomly assigned to four groups (n = 4 per group) receiving an intratumoral injection of 200 µL of the formulations: (i) saline; (ii) NB-shells; (iii) Dox and (iv) NB-shells loaded with Dox. Tumour growth was monitored over a 2-week period. At the end of the treatment period, Dox loaded NB-shell treated mice exhibited almost a 5-fold less tumor volume as compared to the group treated with only saline and an almost 2.5-fold smaller tumor volume as compared to the group treated with native Dox. The tumors almost vanished in the animals treated with Dox loaded NB-shells. This confirmed the tumor inhibitory potency of the Dox loaded NB-shell formulations (Fig. 8A–D). We next evaluated the *in vivo* toxicity of the formulations. Dox loaded NB-shell treated mice did not show any significant change in their body weights after the nanoformulation administration (Fig. 8E) indicating no adverse side effects of the formulations. To further confirm the tumor inhibitory potency of the NB-shells, histological analysis of hematoxylin and eosin (H&E) stained tumor sections was carried out. The data showed a higher amount of dead tissue (shown in the indicated area in Fig. 8F) in Dox loaded NB-shell treated tumors in comparison with other groups, suggesting that Dox loaded NB-shells indeed induced higher cancer cell death in C6 tumor bearing mice.

Taken together, these results demonstrated that in comparison with the free drug, Dox loaded NB-shells demonstrated a significant increase in their *in vivo* anti-tumor activities, intratumoral drug delivery and therapeutic efficacy.

Discussion

The shape of a nanoparticle carries significant importance as this relates to its various physical properties and dictates the particle's fate and its various physiological parameters *i.e.* blood circulation pattern and time, migration ability and interaction with guest molecules.[4,35] Various studies report on the fabrication of non-spherical particles. It is further observed that the shape of a nanoparticle affects its rate of tumor deposition.[35,36] Hence, efforts are on go to generate non-spherical particles carrying superior drug delivery features. Recently, Deotare and his group made poly-methyl methacrylate (PMMA) porous cups synthesized by the electrospray technique.[37] Feringa and co-workers developed bowl-shaped nanoparticles by following molecular motor aggregation technology.[38] Sun and his group synthesized tunable NBs with a precise control of their pore opening by taking advantage of non-covalent interactions such as hydrogen bonding and pi–pi stacking interactions existing between the constituent amphiphilic homopolymers.[39] Im and his group prepared another class of macroporous capsules—polymer shells carrying tunable holes on their surfaces using a polystyrene polymer.[15] Thus, there are many reports which shed light on the usage of different types of polymers towards the synthesis and generation of asymmetric particles with varied morphologies.[10,39,40] Additionally, there are many other exciting classes of nanostructures reported in the literature for effective drug delivery applications. These include Janus nanoparticles,[41] nanogels,[42] nanoshells or core–shell like nanoparticles[38,39] which have proved their worth in the field of biomolecular drug delivery. However, these suffer from many pitfalls. For instance, Janus nanoparticles, due to their unique architecture, are tedious to synthesize. It is also troublesome to gain control over their size, various structural/physical/chemical properties and shape.[41] On the other hand, nanogels fail to generate desirable results owing to their inhomogeneous interior and highly porous structure. This inhomogeneity results in divergencies in their drug encapsulation efficiencies and imparts poor control on their drug release behaviour at the target sites.[42] In addition, various Janus nanoparticles[43] and reported nanoshell based core–shell nanoparticles with a hole or other reported NB like structures are mostly synthesized using long synthetic polymers raising concerns about their *in vivo* safety profiles.[38,39]

Recently peptides, whether large or small, owing to their many unique attributes, have attained the most attractive status towards the fabrication of non-spherical nanostructures. There are many reports, where peptides are used as monomers for the generation of diverse nanomaterials, *i.e.* nanotubes, nanofibers and micellar structures.[44] More significantly, single amino acid-based self-assembled nanostructures have also been shown to provide a simple and easy platform to form a variety of nanostructures.[45]

Hence, this study demonstrated the synthesis and development of stimuli responsive single amino-acid based NB infused-core–shell like microstructures and further attested their utility as pH responsive tumor specific drug delivery systems. The NBs forming the microstructure core here have many attractive properties and advantages over other reported nanoparticles. These include high specific surface areas owing to their concave shape, large pore volume and high drug loading capacity, which endow them with potential drug delivery applications. Owing to their concave nature, the surface area of the NBs can be hypothesized to be significantly larger,
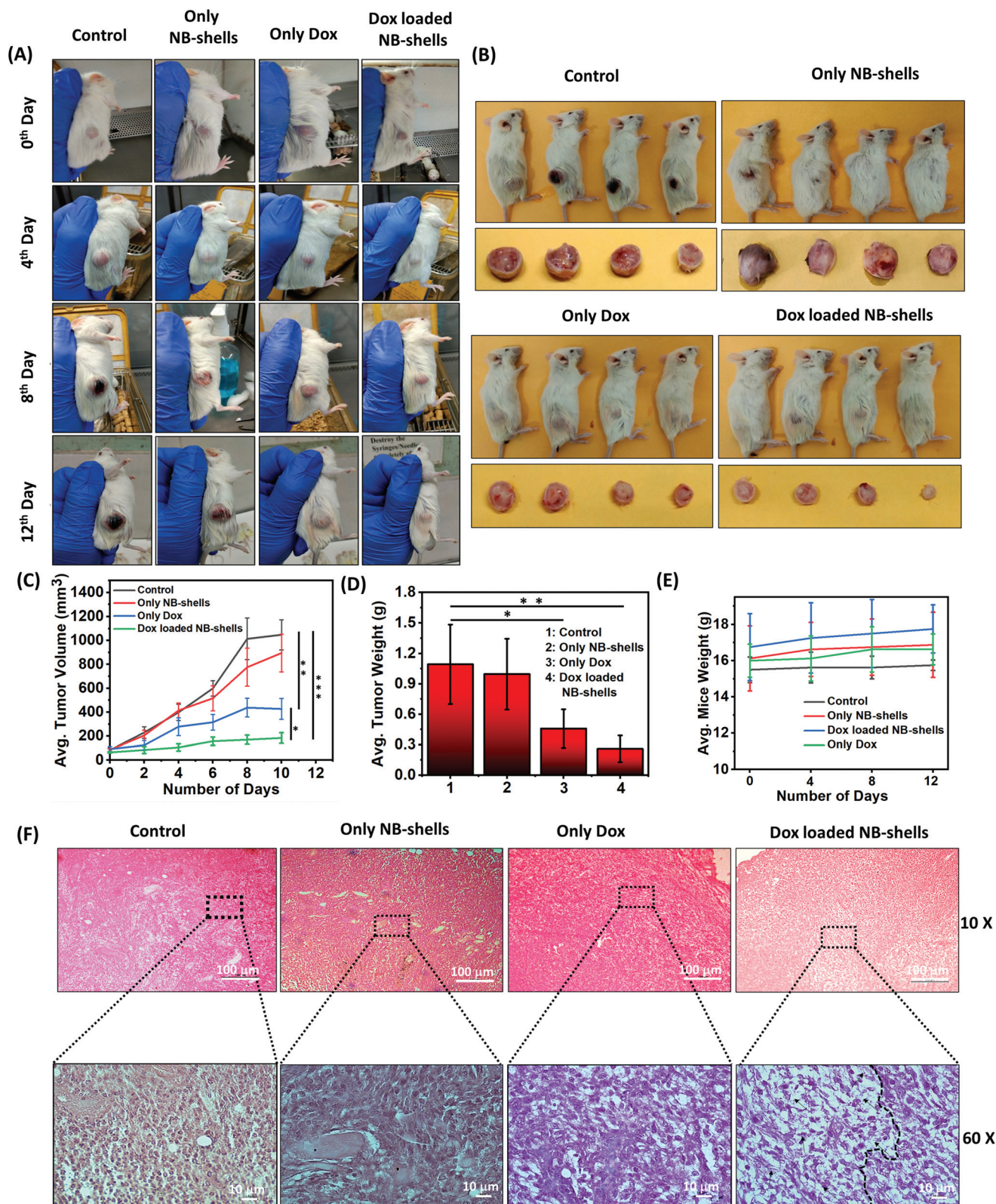
Fig. 8 *In vivo* studies showing the anti-tumor efficacy of Dox loaded NB-shells and free Dox in comparison with the saline-treated control in the mouse model. (A) A digital photograph of mice showing all the groups taken on different days of the study. (B) A digital photograph of tumor bearing mice and the extracted tumor obtained at the end of the treatment *i.e.* at day 14. (C) Tumor volume of the mice taken at different time points on treatment with saline/NB-shells/Dox and Dox loaded NB-shells. (D) Quantitative tumor weight of mice treated with saline/NBs/Dox and Dox loaded NB-shells. (E) Change of the average body weight of mice as a function of time. (F) Histological analysis of tumor sections with H&E staining of the saline/NB-shell/Dox and Dox loaded NB-shell treated group of animals. ***, ** and * represent the levels of significance ($P < 0.001$, $P < 0.01$ and $P < 0.05$, respectively).

while their density is much lower as compared to similar dense solid spherical nanoparticles. This provides them with high drug loading/encapsulation ability as compared to their dense spherical counterparts. Additionally, a mere amino acid-based origin imparts them with high biocompatibility with respect to other long synthetic polymer based asymmetric drug delivery systems.

One major drawback in drug delivery applications is the unwanted premature release of the drug from the nanoparticles when using spherical particles. In our case, the NB core enabled high drug loading due to its shape, and it could also be hypothesized to provide additional support to the outer spherical shell covering providing it an edge over other simple spherical core–shell structures.

We have demonstrated that microfluidics can offer a convenient and minutely controllable route for synthesizing NBs featuring multiple advantages likewise the inclusion of soft lithography to design desired geometries, exploitation of the self-assembly behaviour of single amino-acids to achieve defined structures and further utilization of fluid flow mechanics to tune the particle morphology. The amino acid monomer Cys(Trt)-OH with two different N-terminal modifications, *i.e.* Fmoc-Cys(Trt)-OH and Boc-Cys(Trt)-OH, was chosen as starting material for this study. It was observed that Fmoc-Cys (Trt)-OH formed bowl shaped structures, and Boc-Cys(Trt)-OH resulted in the formation of spherical structures. The self-assembly of the amino-acids was majorly propelled by the non-covalent interactions such as hydrogen bonding, electrostatic and hydrophobic interactions interplaying between the monomer units. The Fmoc moiety present in the amino acid mimetics could be hypothesized to provide additional driving forces for biomolecular self-assembly which facilitated hydrogen bonding among the carbonyl groups,[46] aromatic and hydrophobic interactions in the fluorenyl ring[47,48] and steric interactions from the linker (the methoxy-carbonyl group)[49] contributed together towards the formation of the self-assembled structures. These unique interactions in combination with the driving forces from the amino acid back-bone resulted in the self-assembly of the Fmoc-modified amino acid into a kinetically rapid and thermodynamically rigid phase leading to the formation of particles with a varied shape. It has been earlier observed that many Fmoc modified amino acids and Fmoc-group carrying short peptides possessed relatively fast self-assembly kinetics and presented remarkable physicochemical properties along with manifold uses in a number of fields, including drug delivery and anti-microbial therapeutics to name a few.[47,49,50]

The fact that the NBs were only obtained in the case of the microfluidics-based approach speaks volumes of the technology and the crucial role played by it in the formation of the NBs. Self-assembled NBs formed in our case are both thermodynamically (employing intermolecular interactions) and kinetically (utilizing fluid flow) controlled and are stable structures where monomer molecules interact with each other through the mediation of non-covalent interactions resulting in a core shell-like nanoarchitecture *via* following microfluidics flow synthesis.

Though the mechanism of the formation of the NBs in our case is yet unknown, it could be envisaged here that, the NB formation took place by virtue of the phase interface effect, such as the interfacial reaction and interfacial self-assembly. Basically, interfacial reaction refers to the reaction at the phase interface induced by the interaction between the two phases, for example water and acetone here. We hypothesize that, in our case, the microfluidic flow propelled fast diffusion of water rapidly into the amino acid containing the organic solvent, acetone. This might have resulted in higher accumulation of the Fmoc amino acid at the acetone–water interface (Scheme 3). Sudden phase separation and fast precipitation of the amino acid occurred at this point, which led to solvent release followed by particle self-assembly. Due to the fast flow profile in a microfluidic setup, the water droplet might have been pushed deep into the amino acid molecules present in their corresponding acetone solution leading to invagination and the formation of the resultant bowl-shaped structures.[51] As the reaction proceeded the increased thickness of the shell further inhibited the diffusion process of the reactant mole-
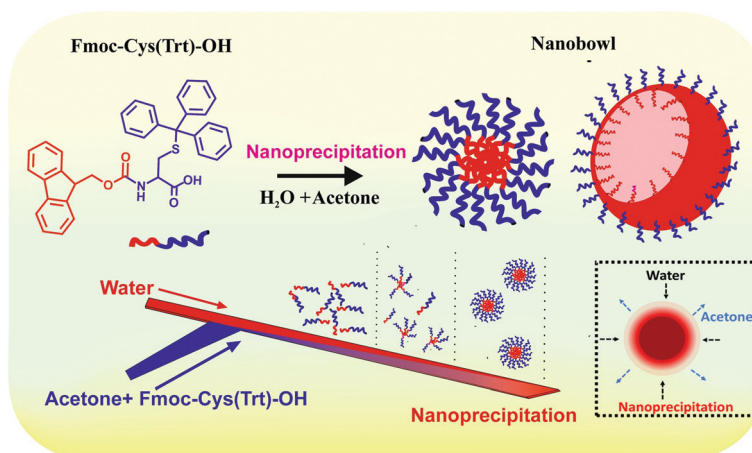
Scheme 3 Mechanism of formation of NBs using microfluidics.

cules across the two phases and ceased the reaction leaving an empty bowl-like structure.[51]

It was interesting to note that, a mere N-terminal modified analogue of Fmoc-Cys(Trt)-OH, *i.e.* Boc-Cys(Trt)-OH, did not show the formation of bowl-shaped particles. Such a difference in the assembly behaviour of the amino acid mimetic with a mere modification in the N-terminal residue is quite exciting and has been previously observed in the case of other peptides and amino acids, where the self-assembly behaviour was decisively altered by varying the end groups.[51,52] Furthermore, it was observed that the particles exhibited concentration dependent assembly behaviour and NBs were obtained at higher amino acid concentrations.

Interestingly, we also observed that the formation of NBs can be tuned by varying microfluidics flow parameters. It was observed that an amino acid concentration of 0.5 mg mL^{-1}, a flow rate of 2 mL min^{-1} and a channel dimension of 100 μm proved to be the most optimum conditions for the generation of the bowl-shaped structures as observed from SEM analysis. Similar concentration-based formation of hollow microparticles was observed in a study by Vasiliauskas *et al.* In their study, the group synthesized different polymeric particles using microfluidic channels created in a PDMS chip with three different polymer types that included acetylated dextran (Ac-Dex), poly(lactic-*co*-glycolic acid) (PLGA) and hypromellose acetate succinate (HPMC-AS). They concluded from their study that the formation of hollow microparticles was independent of the polymer being used.[51]

Following the formation of NBs, one of the most limiting technical challenges was finding a method to completely seal the bowls or open the particles. While open porous nanocontainers allow easy loading of the guest molecules, they must be closed to prevent the leaching and functional activity of the guest molecules. We followed an efficient way to close the pores of NBs by using Boc-Cys(Trt)-OH based shells. In addition, it should be noted that the optimization of a process to generate the NB-infused microparticles (NB-shells) would increase the applicability of the current asymmetric NB based delivery system by protecting the functional molecules inside the hollow core against the harsh environmental conditions. While the detailed mechanism behind the formation of a coating shell on the bowl-shaped particles is not fully understood, major reasons could be the existence of hydrophobic, hydrophilic and pi–pi stacking interactions between the groups of amino acids, *i.e.* Fmoc-Cys(Trt)-OH and Boc-Cys(Trt)-OH comprising the system. Interestingly, the shell coated bowl-shaped particles remained intact at pH 7, but owing to the presence of the acid labile moieties, the formation of pore like openings on the shells was observed at pH 5 and pH 2 (Fig. 5). The formation of acid switchable pores in the NB-shells was further confirmed by the elevated release behaviour of the encapsulated anti-cancer drug Dox from the NB-shells under acidic pH conditions as shown in Fig. 6. The dissociation of the acid labile Boc/Trt group from the structures in acidic pH could be hypothesized to be the reason behind the pore formation and opening of the structures under acidic pH.

Opening of the microstructure pores under acidic pH conditions validates their potential as efficient platforms for stimuli responsive drug delivery that can be further exploited in the direction of achieving site triggered drug delivery in tumor tissues. Similar pH responsive microporous particles were also formed by Homayun *et al.* in 2018, using poly(methacrylic acid-coethyl acrylate) *via* following a solvent swelling–evaporation method.[53]

The formation of porous particles has gained significant interest among pharmaceutical and drug delivery scientists due to their specific properties such as large surface area, high drug loading capacity and low density, which make them suitable candidates as specialized vehicles to be used in the field of drug delivery.[5] Large pore volumes of hollow nanostructures can be used to incorporate various hydrophobic and hydrophilic drugs and release them in a controlled manner at a particular targeted site.[5,32,33,54] In order to establish the potency of the bowl-shaped particles as an effective drug carrier, we extended our studies towards determining the cellular uptake behaviour of the particles. Cellular uptake experiments were carried out in C6 glial cells. Results showed the presence of highly fluorescent cells in groups treated with Dox loaded NB-shells confirming positive uptake and release of the anti-cancer drug inside cells. A similar fluorescence based cellular uptake study of hollow polystyrene particles loaded with coumarin-6 was reported by Im *et al.* in 2005.[15] The uptake study was followed by efficacy studies of the drug loaded NB-shells in C6 cells. It was observed that the NB-shells exhibited an increase in the cytotoxicity of the loaded anti-cancer drug and the highest killing of cells was observed in the case of Dox loaded NB-shells as compared to all other groups at all tested concentrations (Fig. 7). After establishing the particle efficacy in cell lines, we next probed the therapeutic efficacy of the Dox-loaded NB-shells in animal models. It was observed that treatment with Dox loaded NB-shells resulted in significantly retarded tumor growth in glioma tumor-bearing animals as compared to other treatment groups (Fig. 8). The enhanced efficacy achieved in the case of Dox loaded NB-shells could be attributed to their higher cellular uptake and triggered release of the entrapped Dox in tumor tissues caused by the acidic tumor environment, resulting in a high tumor tissue drug payload.[55]

Conclusion

Particle shape is one of the long-neglected geometric parameters in the application of nano-drug delivery systems. Many previous reports, however, made an unchallengeable progress for attaining diversely shaped particles. We in the current work have demonstrated a robust and straightforward procedure to produce bowl-shaped nanoparticles using a flow focusing lithography-based microfluidics device. In this study, a combined methodology based on the merging of microfluidics along with supramolecular self-assembly has been established to obtain bowl-shaped structures using a single amino acid. It

has also been observed here that in the process of generating these microfluidics propelled asymmetric-NB like core–shell structures, the nature of the constituent single amino acid, its end modifications, flow rate parameters in microfluidic channels and concentration of amino acids played vital roles in dictating their self-assembly process and the resultant structure thus formed. The hallmarks of our currently proposed asymmetric nanocomposite drug delivery system include (i) generation of anti-cancer drug loaded bowl-shaped particles engendered using a one-step microfluidics based approach; (ii) infusion of these NBs into a pH-responsive vesicular shell whose opening/closing is tunable by a pH change capable of on-demand anticancer drug delivery mediated by a tumor environment specific pH switch; and (iii) self-assembly of mere amino-acid mimetics into a NB-vesicle composite core shell like microstructure. The structures formed here exhibited a high drug loading capacity and showed a sustained drug release profile for the encapsulated drug. To the best of our knowledge, this is the first report on the fabrication of the bowl-shaped-core–shell particles from a simple amino acid mimetic using a microfluidics-based one-step approach along with its manifestation as a stimuli responsive anti-cancer drug delivery platform in cellular and animal tumor models. Ultimately, our NB-core shell encapsulation system strives to provide a new research area in the development of well turned-out and neatly fabricated drug delivery systems towards solving the major challenges of pH-sensitive cancer therapeutics.

Experimental section

Preparation of a microfluidic device

A detailed description of the synthesis of the microfluidic device is provided in the ESI section (1–4).†

Preparation of particles and NBs

To prepare the particles of Fmoc-Cys(Trt)-OH and Boc-Cys(Trt)-OH using microfluidics, different amounts of amino acids, 0.1 mg, 0.25 mg, and 0.5 mg, were dissolved in acetone and injected into the microreactor at a flow rate of 800 μL min^{-1} from one inlet. Water of milli Q grade was injected at a flow rate of 1200 μL min^{-1} through the second inlet, making a cumulative flow rate of 2 mL min^{-1} at the outlet. On the other hand, manual samples were prepared by first dissolving similar concentrations of amino acids as described above in acetone, followed by initiating the assembly process by adding water.

Particle characterization studies

The mean size and PDI of the self-assembled amino acid-based structures (particles, NBs and NB-shells) were determined by using a dynamic light scattering instrument (Zetasizer Nano ZSP; Model ZEN5600; Malvern Instrument Ltd, Worcestershire, UK). NB-shell stability was also determined for a period of 48 h using DLS.

The morphological features of the amino acid mimetic derived particles were determined by using a JEOL SEM scanning electron microscope. For SEM sample preparation, the particles were first drop cast on silicon wafers, air-dried, and then they were coated with gold for a period of 90 s in an auto fine coater (JEOL JEC-3000FC).

TEM analysis of the particles was performed in a JEOL TEM 2100 instrument with a tungsten filament at 120 kV. This study was performed to determine the morphology of the bowl-shaped particles. The particles prepared through microfluidics and manual methods were diluted equally and then drop cast on 200 nm mesh sized carbon-coated copper grids; subsequently, the samples were stained with 2% (w/v) uranyl acetate. Furthermore, AFM was employed in tapping mode for imaging the particles using a Bruker Nanoscope-V instrument at an optimum scanning frequency of ∼1 Hz with a number of pixels of ∼512. With a cantilever length of 196 μm, the spring constant was selected to be 0.06 N m^{-1} for sample analysis. The samples prepared *via* both microfluidics and manual self-assembly were drop cast on a silicon chip and air-dried for AFM analysis.

Furthermore, to confirm the hollow cavity-like structures of the NBs, we first prepared the NBs using a microfluidics chip and then loaded their hollow cavities with polystyrene beads by incubating them with 10 μL of polystyrene bead dispersion (ESI section 5†). Nanobowls incubated with the beads were briefly sonicated for 15 min for facilitating bead encapsulation and were then kept for overnight incubation. After incubation, the sample was drop cast on silicon wafer for SEM analysis.

Drug encapsulation study

The percentage encapsulation of the drugs in the NBs was determined by using the centrifugation method. Samples taken in amicon filters were centrifuged at 5000 rpm for 45 min and drug loading was determined by taking the absorbance of the sample at 480 nm of Dox. Confocal microscopic analysis was carried out (using Carl Zeiss Microscopy LSM 880) in order to visualize the encapsulated Dox inside the structures. Images were acquired at 100× magnification by using the red channel for Dox. Percentage drug encapsulation inside the NBs was calculated using eqn (1).

$$PE = \frac{I_R - F_R}{I_R} \times 100 \qquad (1)$$

Here, PE, I_R and F_R are percentage encapsulation, initial reading of the drug, and filtrate reading, respectively.

Coating NBs with a pH responsive amino-acid based vesicular shell

After carrying out drug loading inside the NBs, they were coated with a Boc-Cys(Trt)-OH based vesicular shell by following manual self-assembly to form NB-infused core shell like microstructures (NB-shells). Briefly, NBs were collected from the microchannel outlet and coated with Boc-Cys(Trt)-OH. For coating, 5 mg of Boc-Cys(Trt)-OH was first dissolved in a minimum amount of acetone and the acetone solution of Boc-Cys(Trt)-OH was then added to the bowl-shaped particles.

Then the sample pH was adjusted to 7 using 100 mM NaOH solution and it was kept for incubation at room temperature for 1 h. Further characterization studies of NB-shells was performed using DLS, SEM, AFM and confocal microscopy. Stability study of the NB-Shells was also perfomed for a period of 48 h using DLS analysis (ESI section 6†).

Closing and opening of NB-shells at alkaline and acidic pH

After the confirmation of the formation of the NB-shells at pH 7, we next investigated the responsiveness of the microstructures towards varying pH conditions *i.e.* pH 5 and pH 2 by adjusting the pH of the NB-shells with HCl. Structural changes were investigated using DLS, SEM and confocal microscopy.

Confirmation of acid triggered amino acid degradation using HPLC analysis

HPLC combined with mass spectrometry were used to monitor the acid triggered deprotection/dissociation of acid-labile moieties (Trt/Boc) from the amino acid Boc-Cys(Trt)-OH. Details of this are provided in ESI section 8.†

Drug release kinetics study

The release profile of Dox from the NB-shells was monitored at pH 7, pH 5 and pH 2 in respective buffer solutions using the dialysis bag method. Native Dox and NB-shells encapsulating Dox were placed into a dialysis bag (MWCO: 12 kDa) and were dialyzed against 80 mL of buffers maintained at different pH values of 7, 5, and 2 under gentle stirring at 37 °C. At defined time intervals (0.25, 0.5, 1, 2, 4, 6, 8, 24 and 48 h), 1 mL of the released media was taken out for sample analysis, and this was followed by replenishing the churned-out media with an equivalent volume of the fresh dialysing buffer. The quantity of Dox released from the NB-shells was detected by carrying out UV-visible spectrophotometry at 480 nm (using a UV-VIS spectrophotometer, Shimadzu, Japan).

Cellular uptake in C6 (glioma cell lines)

Cellular uptake studies of the drug-loaded samples were carried out in C6 cells (ESI section 10 and 11†). The inherent fluorescence of Dox was exploited to visualize the cells under confocal microscopy. C6 cells were cultured on a 35 mm glass bottom dish and were incubated with the Dox loaded NB-shells for 6 h after which the samples were washed with phosphate buffered saline (PBS) followed by the acquisition of confocal microscopy images at 100× magnification in the red channel for Dox using a confocal microscope.

Before carrying out *cell culture* studies, extensive dialysis of the particles was carried out in PBS in order to get rid of residual acetone, followed by morphological analysis using SEM, which demonstrated the retention of the bowl like structures and the covering after being dialysed for 24 h as shown in ESI section 12 and Fig. S10.†

In vitro efficacy study

C6 cells were plated (5×10^4 cells per well) in triplicate in 96-well sterile microtiter plates and allowed to grow for 24 h, for facilitating proper cell adhesion. The cells were then treated with only Dox, Dox loaded NB-shells and void NB-shells at different concentrations and incubated for 24 h before carrying out cell viability assays. Cells were also incubated with PBS as the control. After incubating the cells with the samples for 24 h, the used media were discarded and replaced with 180 μL of fresh growth media. Then subsequently, 20 μL of MTT 3-(4,5-dimethylthiazol-2-yl)-2,5-diphenyltetrazolium reagent was added to each well. This was followed by incubating the plate for 4 h at 37 °C under 5% CO_2. After completion of the incubation period, the used media were removed from the wells followed by the addition of 100 μL of DMSO to each well to solubilize the formazan crystals. Then sample absorbance was measured at 572 nm.

In vivo efficacy studies in tumour-bearing mice

In vivo animal experiments were performed at the National Centre for Cell Science, Pune, India for approximately 15 days in tumour-bearing mice (weighing 25–30 g). "All animal procedures were performed in accordance with the Guidelines for Care and Use of Laboratory Animals approved by 'Committee for the Purpose of Control and Supervision of Experiments on Animals' (CPCSEA), Government of India, and experiments were approved by Institutional Animal Care and Use Committee (IACUC) of National Centre for Cell Science (NCCS), Pune, India".

Tumor regression studies were carried out in mice bearing C6 glioma tumors. To initiate tumor growth, cells were injected subcutaneously (5×10^5 cells per mL) into the right flank of 4–6 weeks old NOD/SCID tumour-bearing mice. Tumors developed within 12–15 days of injection. After the establishment of tumor masses, the mice carrying tumors were randomly divided into four groups ($n = 4$ in each group) and injected intratumorally with 200 μL of Dox alone and 200 μL of Dox loaded NB-shells in PBS containing an amount of Dox equivalent to 5 mg per kg body weight of the animal, every alternate day for a period of 12 days. Void NB-shells were taken as the vehicle control. The tumor size was measured before the start of the treatment and after every injection using callipers and the volume was calculated using eqn (2)

$$T_v = 0.5 \times (L \times W^2) \tag{2}$$

Here, T_v is the tumor volume. L and W correspond to the length and width of the tumor.

Statistical analysis

Data analysis was performed using Microsoft excel, Origin, and GraphPad Prism Software and represented as mean ± standard deviation to express the data. ANOVA or T-test was used to calculate and compare the differences between the mean values of subgroups. $p \leq 0.05$ was considered statistically significant. ***, ** and * represent the levels of significance ($P < 0.001$, $P < 0.01$ and $P < 0.05$, respectively).

Conflicts of interest

There are no conflicts to declare.

Acknowledgements

References

1 I. Khan, K. Saeed and I. Khan, *Arabian J. Chem.*, 2019, **12**, 908–931.

2 K. Gajanan and S. N. Tijare, *Mater. Today*, 2018, **5**, 1093–1096.

3 O. V. Salata, *J. Nanobiotechnol.*, 2004, **2**, 3.

4 R. Toy, P. M. Peiris, K. B. Ghaghada and E. Karathanasis, *Nanomedicine*, 2014, **9**, 121–134.

5 Y. Si, M. Chen and L. Wu, *Chem. Soc. Rev.*, 2016, **45**, 690–714.

6 S. Venkataraman, J. L. Hedrick, Z. Y. Ong, C. Yang, P. L. R. Ee, P. T. Hammond and Y. Y. Yang, *Adv. Drug Delivery Rev.*, 2011, **63**, 1228–1246.

7 J. A. Champion and S. Mitragotri, *Proc. Natl. Acad. Sci. U. S. A.*, 2006, **13**, 4930–4934.

8 Y. Zhao, Y. Wang, F. Ran, Y. Cui, C. Liu, Q. Zhao, Y. Gao, D. Wang and S. Wang, *Sci. Rep.*, 2017, **7**, 1–11.

9 S. Alam, J. J. Panda, T. K. Mukherjee and V. S. Chauhan, *J. Nanobiotechnol.*, 2016, **14**, 1–4.

10 Z. J. Chen, S. C. Yang, X. L. Liu, Y. Gao, X. Dong, X. Lai, M. H. Zhu, H. Y. Feng, X. D. Zhu, Q. Lu, M. Zhao, H. Z. Chen, J. F. Lovell and C. Fang, *Nano Lett.*, 2020, **20**, 4177–4187.

11 F. Iskandar, A. B. D. Nandiyanto, W. Widiyastuti, L. S. Young, K. Okuyama and L. Gradon, *Acta Biomater.*, 2009, **5**, 1027–1034.

12 W. Tong, X. Song and C. Gao, *Chem. Soc. Rev.*, 2012, **41**, 6103–6124.

13 H. Schiffter, J. Condliffe and S. Vonhoff, *J. R. Soc., Interface*, 2010, **7**, S483–S500.

14 S. Desgouilles, C. Vauthier, D. Bazile, J. Vacus, J. L. Grossiord, M. Veillard and P. Couvreur, *Langmuir*, 2003, **19**, 9504–9510.

15 S. H. Im, U. Jeong and Y. Xia, *Nat. Mater.*, 2005, **4**, 671–675.

16 H. Wen, H. Dong, J. Liu, A. Shen, Y. Li and D. Shi, *J. Mater. Chem. B*, 2016, **4**, 7859–7869.

17 J. Wang, W. Mao, L. L. Lock, J. Tang, M. Sui, W. Sun, H. Cui, D. Xu and Y. Shen, *ACS Nano*, 2015, **9**, 7195–7206.

18 I. F. Uchegbu, *Expert Opin. Drug Delivery*, 2006, **3**, 629–640.

19 L. Wang, C. Gong, X. Yuan and G. Wei, *Nanomaterials*, 2019, **9**, 285.

20 J. K. Patra, G. Das, L. F. Fraceto, E. V. R. Campos, M. del Pilar Rodriguez-Torres, L. S. Acosta-Torres, L. A. Diaz-Torres, R. Grillo, M. K. Swamy, S. Sharma and S. Habtemariam, *J. Nanobiotechnol.*, 2018, **16**, 71.

21 H. Hosoya, A. S. Dobroff, W. H. Driessen, V. Cristini, L. M. Brinker, F. I. Staquicini, M. Cardó-Vila, S. D'Angelo, F. Ferrara, B. Proneth and Y. S. Lin, *Proc. Natl. Acad. Sci. U. S. A.*, 2016, **113**, 1877–1882.

22 L. Xu, P. Frederik, K. F. Pirollo, W. H. Tang, A. Rait, L. M. Xiang, W. Huang, I. Cruz, Y. Yin and E. H. Chang, *Hum. Gene Ther.*, 2002, **13**, 469–481.

23 G. Zhao, S. Chandrudu, M. Skwarczynski and I. Toth, *Eur. Polym. J.*, 2017, **93**, 670–681.

24 F. Clerici, E. Erba, M. L. Gelmi and S. Pellegrino, *Tetrahedron Lett.*, 2016, **57**, 5540–5550.

25 K. Tao, A. Levin, L. Adler-Abramovich and E. Gazit, *Chem. Soc. Rev.*, 2016, **45**, 3935–3953.

26 S. Perween, B. Chandanshive, H. C. Kotamarthi and D. Khushalani, *Soft Matter*, 2013, **9**, 10141–10145.

27 Y. Zhang, H. F. Chan and K. W. Leong, *Adv. Drug Delivery Rev.*, 2013, **65**, 104–120.

28 P. M. Valencia, O. C. Farokhzad, R. Karnik and R. Langer, *Nat. Nanotechnol.*, 2012, **7**, 623–629.

29 J. P. Martins, G. Torrieri and H. A. Santos, *Expert Opin. Drug Delivery*, 2018, **15**, 469–479.

30 H. Zhang, Y. Zhu and Y. Shen, *Small*, 2018, **14**, 1800360.

31 A. Baruah, A. Jindal, C. Acharya, B. Prakash, S. Basu and A. K. Ganguli, *J. Micromech. Microeng.*, 2017, **27**, 035013.

32 R. Bird, T. J. Freemont and B. R. Saunders, *Chem. Commun.*, 2011, **47**, 1443–1445.

33 F. Yu, X. Tang and M. Pei, *Microporous Mesoporous Mater.*, 2013, **173**, 64–69.

34 A. H. Mo, P. B. Landon, K. S. Gomez, H. Kang, J. Lee, C. Zhang, W. Janetanakit, V. Sant, T. Lu, D. A. Colburn and S. Akkiraju, *Nanoscale*, 2016, **8**, 11840–11850.

35 S. Muro, C. Garnacho, J. A. Champion, J. Leferovich, C. Gajewski, E. H. Schuchman, S. Mitragotri and V. R. Muzykantov, *Mol. Ther.*, 2008, **16**, 1450–1458.

36 X. Zhu, C. Vo, M. Taylor and B. R. Smith, *Mater. Horiz.*, 2019, **6**, 1094–1121.

37 P. B. Deotare and J. Kameoka, *Nanotechnology*, 2006, **17**, 1380–1383.

38 L. E. Franken, Y. Wei, J. Chen, E. J. Boekema, D. Zhao, M. C. Stuart and B. L. Feringa, *J. Am. Chem. Soc.*, 2018, **140**, 7860–7868.

39 H. Sun, D. Liu and J. Du, *Chem. Sci.*, 2019, **10**, 657–664.

40 P. Li, K. Pan and J. Deng, *Nanoscale*, 2019, **11**, 23197–23205.

41 L. T. Tran, S. Lesieur and V. Faivre, *Expert Opin. Drug Delivery*, 2014, **11**, 1061–1074.

42 Y. Yin, B. Hu, X. Yuan, L. Cai, H. Gao and Q. Yang, *Pharmaceutics*, 2020, **12**, 290.

43 B. Shaghaghi, S. Khoee and S. Bonakdar, *Int. J. Pharm.*, 2019, **559**, 1–2.

44 N. Habibi, N. Kamaly, A. Memic and H. Shafiee, *Nano Today*, 2016, **11**, 41–60.

45 N. Gour, P. C. Kanth, B. Koshti, V. Kshtriya, D. Shah, S. Patel, R. Agrawal-Rajput and M. K. Pandey, *ACS Chem. Neurosci.*, 2018, **10**, 1230–1239.

46 S. Fleming, P. W. Frederix, I. Ramos Sasselli, N. T. Hunt, R. V. Ulijn and T. Tuttle, *Langmuir*, 2013, **29**, 9510–9515.

47 A. Mahler, M. Reches, M. Rechter, S. Cohen and E. Gazit, *Adv. Mater.*, 2006, **18**, 1365–1370.

48 A. M. Smith, R. J. Williams, C. Tang, P. Coppo, R. F. Collins, M. L. Turner, A. Saiani and R. V. Ulijn, *Adv. Mater.*, 2008, **20**, 37–41.

49 S. Fleming, S. Debnath, P. W. Frederix, T. Tuttle and R. V. Ulijn, *Chem. Commun.*, 2013, **49**, 10587–10589.

50 S. Fleming and R. V. Ulijn, *Chem. Soc. Rev.*, 2014, **43**, 8150–8177.

51 R. Vasiliauskas, D. Liu, S. Cito, H. Zhang, M. A. Shahbazi, T. Sikanen, L. Mazutis and H. A. Santos, *ACS Appl. Mater. Interfaces*, 2015, **7**, 14822–14832.

52 A. Dolid and M. Reches, *J. Pept. Sci.*, 2019, **25**, e3212.

53 B. Homayun, C. Sun, A. Kumar, C. Montemagno and H. J. Choi, *Eur. J. Pharm. Biopharm.*, 2018, **128**, 316–326.

54 K. Cheng, Y. Zhang, Y. Li, Z. Gao, F. Chen, K. Sun, P. An, C. Sun, J. Yong and B. Suna, *J. Mater. Chem. B*, 2019, **7**, 3291–3302.

55 B. Chen, W. Dai, B. He, H. Zhang, X. Wang, Y. Wang and Q. Zhang, *Theranostics*, 2017, **7**, 538.